

1 **Enhancing the Strength of Tissue Paper through Pulp**

2 **Fractionation and Stratified Forming**

3
4 Jérémie Viguié,^{a,b*}, Saurabh Kumar^b, Bruno Carré^b, Laurent Orgéas^c

6 **ABSTRACT**

7 The potential of combining stratified paper forming with pulp fractionation was investigated to
8 improve the balance between low density, which enhances water absorbency and softness, and
9 the dry strength of tissue papers. The selected fractionation approaches allowed us to separate
10 especially stiff, low-fibrillated fibers (A fractions) from flexible, fibrillated fibers containing
11 fines (detached segments of fibers, fibrils, or lamellae fragments) (B fractions). After
12 characterizing the morphological properties of each fiber fraction, 20 g/m² model papers were
13 produced with and without wet pressing to tune the paper density. At a density of 0.3 g/cm³, the
14 **tensile breaking stress** of B papers was at least three times higher than that of A papers. The
15 **strain at break** of B papers was also close to two times higher than that of A papers.
16 Interestingly, bilayer papers AB exhibited **breaking stress** values intermediate between those of
17 A and B papers, while native pulp papers, *i.e.*, without fractionation and stratified forming,
18 followed the trend of A papers. Notably, bi-layering the paper improved the **breaking stress** by
19 up to twice as much without increasing the paper density, which could be highly beneficial in
20 improving the balance of properties in tissue paper grades.

21
22 *Keywords: stratified forming, pulp fractionation, mechanical strength, tissue paper*

23
24 *Contact information:*

25 *a: Univ. Grenoble Alpes, CNRS, Grenoble INP, LGP2, F-38000 Grenoble, France*

26 *b: Centre Technique du Papier (CTP), F-38044 Grenoble, France*

27 *c: Univ. Grenoble Alpes, CNRS, Grenoble INP, 3SR Lab, F-38000 Grenoble, France*

28
29 **Corresponding author: jeremie.viguie@lgp2.grenoble-inp.fr*

31 **1. INTRODUCTION**

32 Environmental and economic concerns are driving manufacturers of tissue papers to
33 minimize the production resources (raw materials, energy, water...) while optimizing the end-
34 use performances of these particular papers. Meanwhile, tissue papers require a combination of

35 different properties to be increased and optimized: **mechanical in-plane strength in both dry and**
36 **wet states**, water absorbency, out-of-plane bulk and surface softness's (De Assis et al. 2018).
37 This optimization is complex and demands several challenges to be overcome. Indeed, the fiber
38 web features that are optimal for providing high mechanical strength unfortunately greatly
39 differ from those required for high absorbency and softness. For example, refining the pulp or
40 adding of micro-fibrillated cellulose are known processing routes used to increase the in-plane
41 strength of tissue papers by increasing the density of the fiber network and by improving
42 bonding between fibers. However, in the same time, such forming techniques alter the
43 absorbency and the (bulk and surface) softness of corresponding papers (Gigac and Fišerová
44 2008, Kullander et al. 2012, Wang 2019, Morais et al. 2021a, Morais et al. 2021b, Zambrano
45 et al. 2021, Viguíe et al. 2022). Paper creping acts in the opposite way by delaminating the fiber
46 networks (thus by increasing their porosity and the out-of-plane softness) and by forcing the
47 fiber bonds to be damaged/broken (thus by reducing both their in-plane stiffness and their yield
48 strength) (De Assis et al., 2020).

49 Thus, to circumvent these bottlenecks and to make tissue grades with combined and
50 optimized properties, stratified forming is a possible and relevant processing route which is
51 followed for decades. This method consists in layering different pulps before dewatering using
52 a stratified headbox (Lloyd 2000). Generally, two layers (rarely three) are superimposed. The
53 first/inner layer may be made of long, flexible, highly fibrillated fibers and fines (which are
54 detached segments of fibers, fibrils or lamellae fragments), to improve bonding and thus to
55 provide strength. The second/outer layer(s) may be made of short, stiff and low fibrillated fibers
56 to improve the surface softness as well as the water absorbency capacity (De Assis et al. 2018).
57 Each pulp has a dedicated pulping, cleaning and refining process. Nevertheless, the production
58 cost could be further reduced by using a single type of pulp and by employing pulp fractionation
59 to create distinct groups of fibers with different properties, which could then be used to form
60 the stratified structure.

61 Indeed, stratified forming with prior pulp fractionation was proved to be a good way to
62 optimize the compromise between the production cost and the mechanical performances of
63 graphic papers (Harwood 1990, Oksanen et al. 2012, Huber et al. 2013). The controlled
64 distribution of the different fiber fractions through the thickness of the structure by stratified
65 forming has significantly improved the specific bending stiffness of these papers. Fractionation
66 of pulp suspensions can be performed by pressure screening systems or hydrocyclone
67 technologies. Screening systems equipped with finely perforated plates (either slots or holes)
68 fractionate pulp suspensions based on the fiber length. Hydrocyclones fractionate the pulp on

69 the basis of the stiffness and extent of development of fibers (related to wall thickness,
 70 coarseness and fibrillation), resulting from their different fiber migration behavior in the
 71 centrifugal flow field (Huber et al. 2018).

72 To date, no academic work has investigated the potential of stratified forming combined
 73 with pulp fractionation to improve the compromise of properties of tissue papers. This is the
 74 aim of this work: we examine the evolution of the structural and mechanical properties of model
 75 tissue papers processed with softwood kraft pulp, by using both fractionation approaches and
 76 stratification.

77

78 2. EXPERIMENTAL PROCEDURE

79

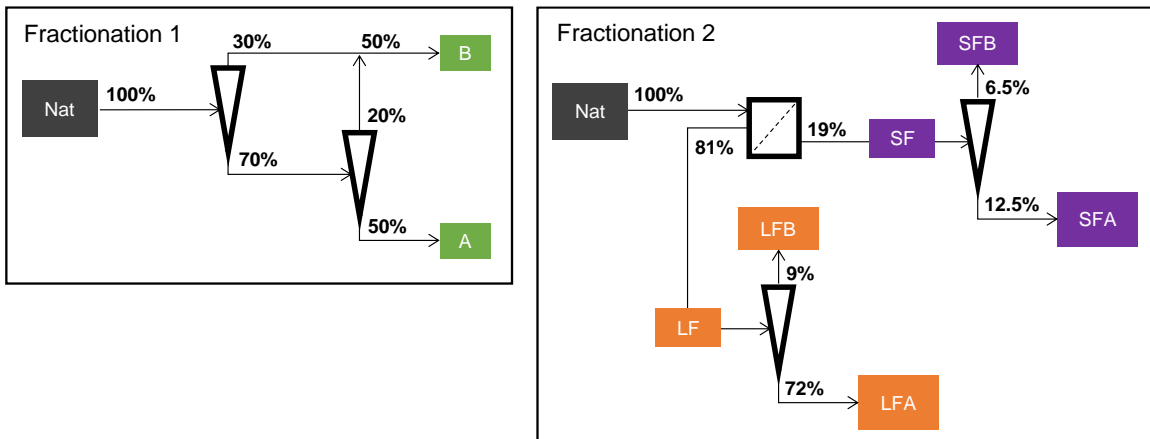
80 2.1. Native Fiber Pulp

81 The native paper pulp was a 100% Northern Bleached Softwood Kraft Pulp (NBSK). It
 82 was slushed in a low consistency pulper (5% consistency, 30 min, 45°C). The pulp had an initial
 83 drainage index of 13°SR. No wet-end additives were used.

84

85 2.2. Pulp fractionation

86 As illustrated in Fig.1, we used two distinct fractionation approaches described
 87 hereafter.



88

89 **Fig. 1** – Schemes of the studied fractionation processes. *Nat* = Native pulp, *A* = Apex fraction, *B* = Base
 90 fraction, *LF* = Long Fiber fraction, *SF* = Short Fiber fraction, *LFA* = Long Fiber Apex fraction, *LFB* =
 91 Long Fiber Base fraction, *SFA* = Short Fiber Apex fraction and *SFB* = Short Fiber Base fraction. **The**
 92 **percentage corresponds to the proportion of dry mass for each obtained fraction.**

93 2.2.1. First fractionation approach

94 The first approach (noted 1) consisted of a two-stage feed-forward hydrocyclone
 95 fractionation. The hydrocyclone fractionation is known to separate fibers following how they

96 migrate in the centrifugal flow field: flexible fibrillated fibers and fines concentrate in the
97 secondary vortex to be collected in the base part of the hydrocyclone while stiff and low
98 fibrillated fibers concentrate in the primary flow to be collected in the apex part (Bergström
99 2006, Huber et al. 2018). This was achieved with an 80 mm head diameter industrial
100 fractionating hydrocyclone (NOSS AM80H). The two-stage feed forward fractionation was
101 performed batch-wise, with the same single hydrocyclone being used for both the stages. Due
102 to limited storage capacity, the first stage hydrocyclone base fraction was thickened on the pilot
103 vacuum disc filter. The filter offers high fiber and fines retention. This thickened base fraction
104 was added to the second stage base fraction to get a combined base fraction (noted B) and then
105 thickened on the same vacuum filter. The other fraction, *i.e.*, the apex fraction (noted A), was
106 collected and thickened using a laboratory centrifugation device, hence retaining all cellulosic
107 elements. **The fractionation parameters were carefully adjusted to achieve a 50% dry mass for**
108 **both the A and B fractions.**

109 2.2.2. Second fractionation approach

110 The second approach (noted 2) consisted in separating the long fibers (LF) from the
111 short ones (SF) by using an industrial pilot pressure screening system equipped with micro-
112 holes basket (0.25 mm) and a 3-element solid core rotor (CTP, France). **Long fibers are defined**
113 **as those that do not pass through the screening system, while short fibers are those that do.** Then
114 each fraction was fractionated in a hydrocyclone. Four new fractions were collected (see Fig.
115 1), *i.e.*, long, stiff and low fibrillated fibers (LFA), long flexible and highly fibrillated fibers
116 (LFB), short stiff and less fibrillated fibers and fines (SFA), short flexible and highly fibrillated
117 fibers and fines (SFB).

118

119 2.3. Manufacturing of model papers

120 Monolayered and stratified model papers were produced using an automated dynamic
121 handsheet former (Techpap, Grenoble, France). The sheet was formed by the projection of pulp
122 on a wire positioned on a rotating cylindrical jar. The wire was completely submerged in a
123 water wall. The pulp projection was accomplished using an injector nozzle fixed on a delivery
124 tube sweeping vertically up and down inside the rotating cylindrical jar. For the stratified model
125 papers, each fraction was projected one after the other. A scoop system bailed out the water
126 wall after the sheet was formed and the water remaining in the sheet was drained by centrifugal
127 force. Sheets were all manufactured with a 20 ± 2 g/m² grammage together with a 0.652 ratio
128 of jet speed/wire speed (wire speed = 920 m/min), so that the fibers were preferentially oriented
129 along the machine direction (MD) rather than along the cross direction (CD). The Sheets, with

130 in-plane dimensions 880 x 240 mm², were slightly pressed to be removed from the wire using
131 a cylindrical roll of 500 g. It is important to note that the longer dimension aligned with the
132 MD, while the shorter dimension aligned with the CD. The sheets were then air-dried without
133 any applied pressure, with the long edges sandwiched between PVC plates, leaving the short
134 edges free.

135 To tailor the paper density, some of the handsheets were further pressed before drying
136 on a roll press with a pressure of 60 N.cm⁻¹ (Techpap, France). They are referred to as “P” in
137 the following. Note that the model papers were not creped. It might be an issue to conclude on
138 the actual effects on the tissue paper (*i.e.*, creped paper). However, De Assis et al. (2020)
139 recently found a reasonable correlation between the performances of uncreped and creped
140 handsheets.

141 Two types of stratified papers have been made: the Stratified 1 with a layer of A fraction
142 and a layer of B fraction, and the Stratified 2 with a layer of mixed LFA and SFA fractions and
143 a layer of mixed LFB and SFB fractions in order to form two independent layers: one with stiff
144 and low-fibrillated fibers and another with flexible, high-fibrillated fibers and fines. Each
145 fraction was added according to its share in the entire pulp (Fig. 1).

146

147 2.4. Characterization methods

148 2.4.1. Morphological properties of fibers

149 The morphological properties of fibers, namely the mean fiber length, the mean fiber
150 width, the coarseness, the fine content and the macrofibrillation index, were measured with a
151 Morfi fiber analyzer (Techpap, France) through image analysis. Note that the macrofibrillation
152 index, which characterizes the external fibrillation of paper fibers, represents the ratio of total
153 fibrils length to the total fiber+fibrils length (down to a scale of 3 μm). Fines are defined as
154 elements with a length of less than 200 μm. Note that here fines were only generated during
155 pulp production since the pulp was not refined (*i.e.*, they are “primary” fines).

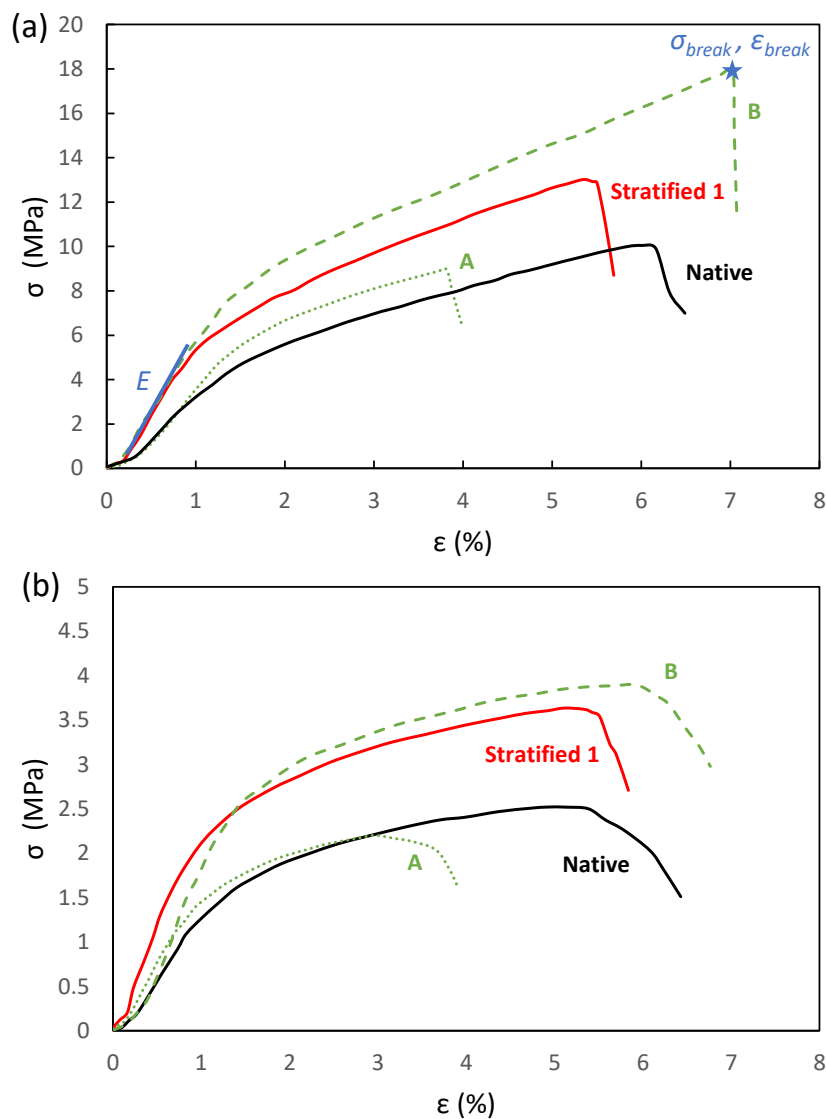
156 2.4.2. Paper sheet physical properties

157 The paper sheet physical properties were assessed using the following standard
158 methods: pre-conditioning (NF EN 20 187, 1993), basis weight (NF EN ISO 536, 1996),
159 thickness adapted to tissue paper (ISO 12625-3) (Vieira et al. 2020) and dry tensile properties
160 adapted to tissue paper (ISO 12625-4). This standard specifies a sample width of 50 mm and a
161 testing speed of 50 mm/min. In our case, the sample length was set to 100 mm, as it was not
162 possible to prepare samples of greater length. It should be noted that the testing conditions
163 deviate from the assumption of pure uniaxial tension. As a result, the elastic modulus, calculated

164 from the slope of the initial linear region of the stress-strain curve, should be considered as an
 165 apparent Young's modulus (noted E). Representative stress-strain curves for some model
 166 papers are presented in Figure 2.

167 2.4.3. Paper sheet microstructures

168 The microstructures of paper sheets were characterized using a field emission scanning
 169 electron microscope (FESEM, model Quanta 200 FEI) with an accelerating voltage of 10 kV.
 170 For that purpose, the samples were mounted onto a substrate with carbon tape and coated with
 171 a thin layer of carbon.



172 **Fig 2.** Representative stress-strain curves for selected model papers under pressed conditions,
 173 tested in (a) MD and (b) CD. E refers to the apparent Young's modulus, σ_{break} denotes the tensile
 174 breaking stress, and ϵ_{break} represents the strain at break.

175

176 **3. RESULTS**

178 **3.1. Structural properties of fibers and model papers**

179 Table 1 reports the morphological properties of the Native and fractionated fibers following
 180 Approach 1. As expected, fraction *B* mainly gathered fibrillated fibers and fines. The external
 181 fibrillation of *B* fibers was twice as high as the external fibrillation of *A* fibers and the fines
 182 content was close to four times higher in fraction *B*. Besides, the fibers of fraction *A* were on
 183 average 25% longer and 15% thicker than the fibers of fraction *B*. Their coarseness was also
 184 15% higher. As a result, the fibers of fraction *A* were expected to be stiffer. Note that the
 185 morphological parameters of the native fibers were in between those reported for fractions *A*
 186 and *B*, as expected.

187 The structural properties of the model **monolayered** papers produced from fractions *A* and *B* are
 188 also reported in Table 1. The fraction *B*, *i.e.*, with more flexible and fibrillated fibers and a
 189 higher content of fines, formed 15% thinner and thus denser fibrous networks, *i.e.*, 134 vs 116
 190 kg/m³ or 288 vs 265 kg/m³ without or with pressing during the paper sheet fabrication,
 191 respectively. At fixed pressing condition, the densification as well as the development of
 192 bonding between fibers during drying are driven by capillary forces that arise from water which
 193 seek to minimize their liquid/air interface (Wohlert et al. 2021). The presence of small elements
 194 like fibrils and fines, as well as the ability of the fiber wall to deform, drastically increase the
 195 surface area subjected to capillary pressure and thus enhance the densification effect and fiber-
 196 to-fiber bonding. In addition, the densification of fibrous media with high polydispersity
 197 (because of the fine content) is also more efficient than that of more monodisperse media.

198
 199 **Table 1.** Morphological properties of fibers of the native pulp, the apex fraction *A*, and the base
 200 fraction *B*, and physical properties of corresponding model **monolayered** papers made under
 201 wet unpressed (UP) or pressed (P) conditions.

	Fractionation 1					
Pulp properties	Native		A (50%)		B (50%)	
Fiber length <i>l</i> (μm)	1298	± 6	1403	± 12	1098	± 10
Fiber width <i>w</i> (μm)	29.1	± 0.1	32.4	± 0.1	28.2	± 0.1
<i>Aspect ratio</i> <i>l/w</i>	45		43		39	
Coarseness (mg/m)	0.14	± 0.01	0.15	± 0.01	0.13	± 0.01
Fibrillation index (%)	0.35	± 0.01	0.30	± 0.01	0.62	± 0.02
Fines content (%)	2.4	± 0.3	1.4	± 0.1	5.5	± 0.2
Paper Properties	UP	P	UP	P	UP	P
Basis weight (g/m ²)	21.3	21.6	21.3	20.7	21.9	23.5
	± 0.2	± 0.2	± 0.5	± 0.6	± 0.4	± 0.3

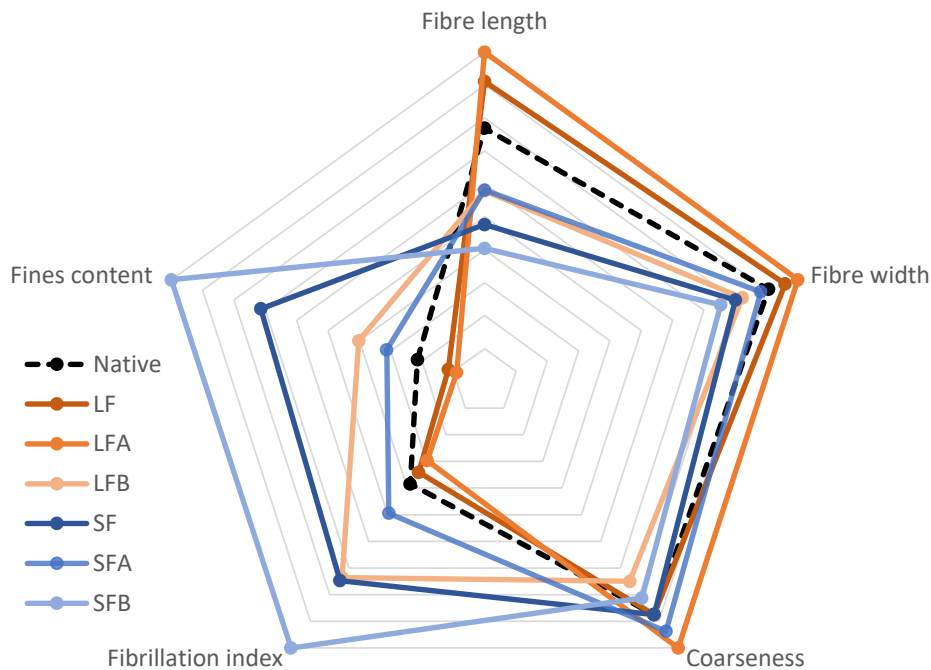
Thickness (μm)		187 ± 5	73 ± 3	184 ± 9	78 ± 4	164 ± 10	83 ± 7
Density (kg/m^3)		114 ± 4	297 ± 14	116 ± 8	265 ± 14	134 ± 9	288 ± 16
RBA (from Eq. 1)		0.07	0.11	0.07	0.08	0.07	0.20
Apparent Young's modulus E (GPa)	MD	0.19 ± 0.04	0.70 ± 0.10	0.17 ± 0.08	0.43 ± 0.12	0.13 ± 0.02	1.00 ± 0.06
	CD	0.05 ± 0.01	0.38 ± 0.08	0.06 ± 0.02	0.22 ± 0.04	0.05 ± 0.01	0.36 ± 0.01
Tensile breaking stress σ_{break} (MPa)	MD	1.84 ± 0.12	9.01 ± 0.67	1.89 ± 0.59	6.73 ± 0.67	5.09 ± 0.32	18.38 ± 0.86
	CD	0.67 ± 0.05	3.03 ± 0.25	0.52 ± 0.2	2.44 ± 0.21	1.20 ± 0.09	5.39 ± 0.22
Strain at break ϵ_{break} (%)	MD	3.6 ± 0.8	5.4 ± 1.3	2.9 ± 0.6	4.2 ± 0.7	5.9 ± 0.7	7.2 ± 1.1
	CD	3.8 ± 0.6	4.6 ± 0.4	2.3 ± 0.4	2.8 ± 0.6	3.7 ± 0.9	6.0 ± 0.9

202
203 Table 2 presents the morphological parameters of fractionated fibers following Approach 2,
204 alongside the structural properties of the related papers. As anticipated, fraction *LF*
205 concentrated long, thick, and low-fibrillated fibers, whereas fraction *SF* concentrated short,
206 thin, highly fibrillated fibers, along with fines. This distribution is visually depicted in Fig. 3.
207 On average, the fibers of fraction *LF* were twice as long and 20% thicker compared to *SF* fibers.
208 Additionally, the external fibrillation of *SF* fibers was at least twice as high as that of *LF* fibers,
209 with *SF* containing at least six times more fines. The hydrocyclone fractionation process applied
210 to each fraction resulted in fraction *LFA*, with the longest and thickest fibers, the lowest
211 fibrillation index, and the lowest fines content. Consequently, fraction *LFA* formed the papers
212 with the lowest densities ($114 \text{ kg}/\text{m}^3$ (UP), $290 \text{ kg}/\text{m}^3$ (P)), while *LF* paper densities were only
213 slightly higher ($120 \text{ kg}/\text{m}^3$ (UP), $302 \text{ kg}/\text{m}^3$ (P)), consistent with the similarities in fiber
214 morphological properties among these groups. Notably, the density of native paper
215 approximated that of *LFA* papers ($114 \text{ kg}/\text{m}^3$ (UP), $297 \text{ kg}/\text{m}^3$ (P)), a result which is possibly
216 attributed to the complex structural properties of a web from mixed fibers. The density of such
217 a web formed from a mixture of conformable and fibrillated fibers with stiff and low-fibrillated
218 fibers could be limited by the stiffer furnish component (Fernandez and Young 1994, Niskanen
219 and Kärenlampi 1998).

220 Fraction *LFB* was characterized by fibers with intermediate length and width, the lowest
221 coarseness, and a relatively high fibrillation index. *SFA* fibers had mean length and width
222 comparable to *LFB* but exhibited higher coarseness and a lower fibrillation index. Networks
223 formed by *LFB* and *SFA* significantly differed in terms of density (156 vs $124 \text{ kg}/\text{m}^3$ (UP), 381
224 vs $319 \text{ kg}/\text{m}^3$ (P)), underscoring the substantial impact of fibrillation index and coarseness on
225 paper density. Finally, *SFB* contained the shortest and thinnest fibers with the highest

226 fibrillation index and fine content, resulting in the formation of paper with the highest density
 227 (218 kg/m³ (UP), 435 kg/m³ (P)). These observations align with existing literature, where
 228 densification is primarily driven by capillary forces during water removal. Specifically, a higher
 229 fibrillation index correlates with increased specific surface area and a decrease of the
 230 characteristic pore sizes, thus enhancing capillary forces and densification. Additionally, mean
 231 coarseness is inversely correlated with paper density. Greater coarseness is associated with
 232 thicker fiber walls, resulting in higher stiffness and ultimately, a less densely packed network.
 233 **Table 2.** Morphological properties of fibers of the long fibers fraction (*LF*), the long fibers apex
 234 fraction (*LFA*), the long fibers base fraction (*LFB*), the short fibers fraction (*SF*), the short fibers
 235 apex fraction (*SFA*) and the short fibers base fraction (*SFB*). Physical properties of model
 236 **monolayered** papers made under wet unpressed (UP) or pressed (P) conditions.

		Fractionation 2											
Pulp properties		LF (81%)		LFA (72%)		LFB (9%)		SF (19%)		SFA (12.5%)		SFB (6.5%)	
Fiber length <i>l</i> (μm)		1537 ± 18		1687 ± 8		977 ± 10		804 ± 4		981 ± 9		682 ± 4	
Fiber width <i>w</i> (μm)		30.8 ± 0.1		32.1 ± 0.1		26.4 ± 0.1		25.7 ± 0.1		28.3 ± 0.1		24.2 ± 0.2	
<i>Aspect ratio l/w</i>		50		53		37		31		35		28	
Coarseness (mg/m)		0.14 ± 0.01		0.16 ± 0.01		0.12 ± 0.01		0.14 ± 0.01		0.15 ± 0.01		0.13 ± 0.01	
Fibrillation index (%)		0.31 ± 0.01		0.27 ± 0.01		0.67 ± 0.01		0.68 ± 0.02		0.45 ± 0.01		0.91 ± 0.01	
Fines content (%)		1.3 ± 0.1		1.0 ± 0.0		4.5 ± 0.3		8.0 ± 0.1		3.5 ± 0.1		11.2 ± 0.2	
Paper Properties		UP	P	UP	P	UP	P	UP	P	UP	P	UP	P
Basis weight (g/m ²)		22.2 ± 0.7	22.5 ± 0.4	20.3 ± 0.9	20.7 ± 0.1	22.6 ± 0.5	22.1 ± 0.8	21.5 ± 1.0	22.0 ± 1.0	21.3 ± 0.2	24.8 ± 1.1	22.8 ± 1.0	21.5 ± 0.6
Thickness (μm)		186 ± 5	76 ± 5	178 ± 9	72 ± 3	145 ± 5	58 ± 3	144 ± 7	64 ± 6	172 ± 10	78.2 ± 7	105 ± 12	50 ± 2
Density (kg/m ³)		120 ± 6	302 ± 16	114 ± 2	290 ± 14	156 ± 3	381 ± 16	149 ± 7	345 ± 18	124 ± 9	319 ± 13	218 ± 18	435 ± 22
RBA (from Eq. 1)		0.06	0.09	0.05	0.06	0.12	0.15	0.14	0.17	0.08	0.11	0.16	0.20
Apparent Young's Modulus <i>E</i> (GPa)	MD	0.16 ± 0.03	0.61 ± 0.08	0.08 ± 0.01	0.43 ± 0.01	0.36 ± 0.02	0.96 ± 0.12	0.41 ± 0.07	0.99 ± 0.09	0.10 ± 0.03	0.59 ± 0.01	0.50 ± 0.06	1.21 ± 0.12
	CD	0.05 ± 0.01	0.43 ± 0.02	0.03 ± 0.00	0.16 ± 0.01	0.15 ± 0.01	0.53 ± 0.05	0.11 ± 0.03	0.51 ± 0.05	0.04 ± 0.01	0.23 ± 0.03	0.21 ± 0.02	0.52 ± 0.04
Tensile breaking stress σ_{break} (MPa)	MD	1.88 ± 0.06	8.45 ± 1.48	1.32 ± 0.07	6.68 ± 0.15	8.30 ± 0.38	28.08 ± 3.47	7.67 ± 0.51	25.30 ± 2.16	2.44 ± 0.41	9.19 ± 0.39	14.39 ± 0.53	36.98 ± 1.44
	CD	0.65 ± 0.05	3.04 ± 0.16	0.46 ± 0.04	2.31 ± 0.26	2.13 ± 0.26	7.15 ± 0.16	1.81 ± 0.22	5.85 ± 0.35	0.78 ± 0.02	3.64 ± 0.50	4.28 ± 0.28	9.76 ± 0.28
Strain at break ϵ_{break} (%)	MD	3.0 ± 0.6	3.6 ± 0.8	2.9 ± 0.7	4.6 ± 0.6	5.9 ± 0.6	7.2 ± 0.4	6.5 ± 0.6	7.8 ± 0.7	5.5 ± 1.0	5.8 ± 1.4	7.0 ± 2.0	6.5 ± 0.9
	CD	3.4 ± 0.4	3.0 ± 0.2	3.8 ± 0.7	4.1 ± 0.8	6.1 ± 0.9	6.3 ± 0.3	5.8 ± 0.8	5.2 ± 0.8	5.5 ± 0.9	4.9 ± 0.5	5.6 ± 1.1	5.6 ± 1.1



238

239 **Fig 3.** Comparison of the dimensionless morphological property for native pulp elements and
 240 the different fractionized pulps obtained from Approach 2. Each dimensionless property value
 241 was calculated as the ratio of the value for the respective fraction to the highest measured value.
 242

243 Table 3 presents the average structural properties of the stratified papers. The mean
 244 density of these papers exhibited some variations compared to that of the Native paper, which
 245 is ascribed to different placements of the various fibrous elements during processing of the
 246 Native paper or the stratified ones. Specifically, it tended to be higher for Stratified 1 (A/B)
 247 paper under unpressed conditions (140 vs. 114 kg/m³) and lower in the pressed configuration
 248 (267 vs 297 kg/m³), along with Stratified 2 (LFA+SFA/LFB+SFB) paper. FESEM images of
 249 the Stratified 1 paper are depicted in Figure 4. The two layers are distinctly visible, with fibers
 250 appearing more densely packed and bonded in the B fraction layer. Additionally, the formation
 251 of bridges composed of fibrils and fines between fibers is evident in the B layer. These
 252 observations correspond to the density contrast between the A and B papers. As already
 253 mentioned, the high polydispersity of the B fraction facilitates densification and bonding, while
 254 fibrils and fine elements increase the specific surface area exposed to capillary pressure, further
 255 enhancing these effects.

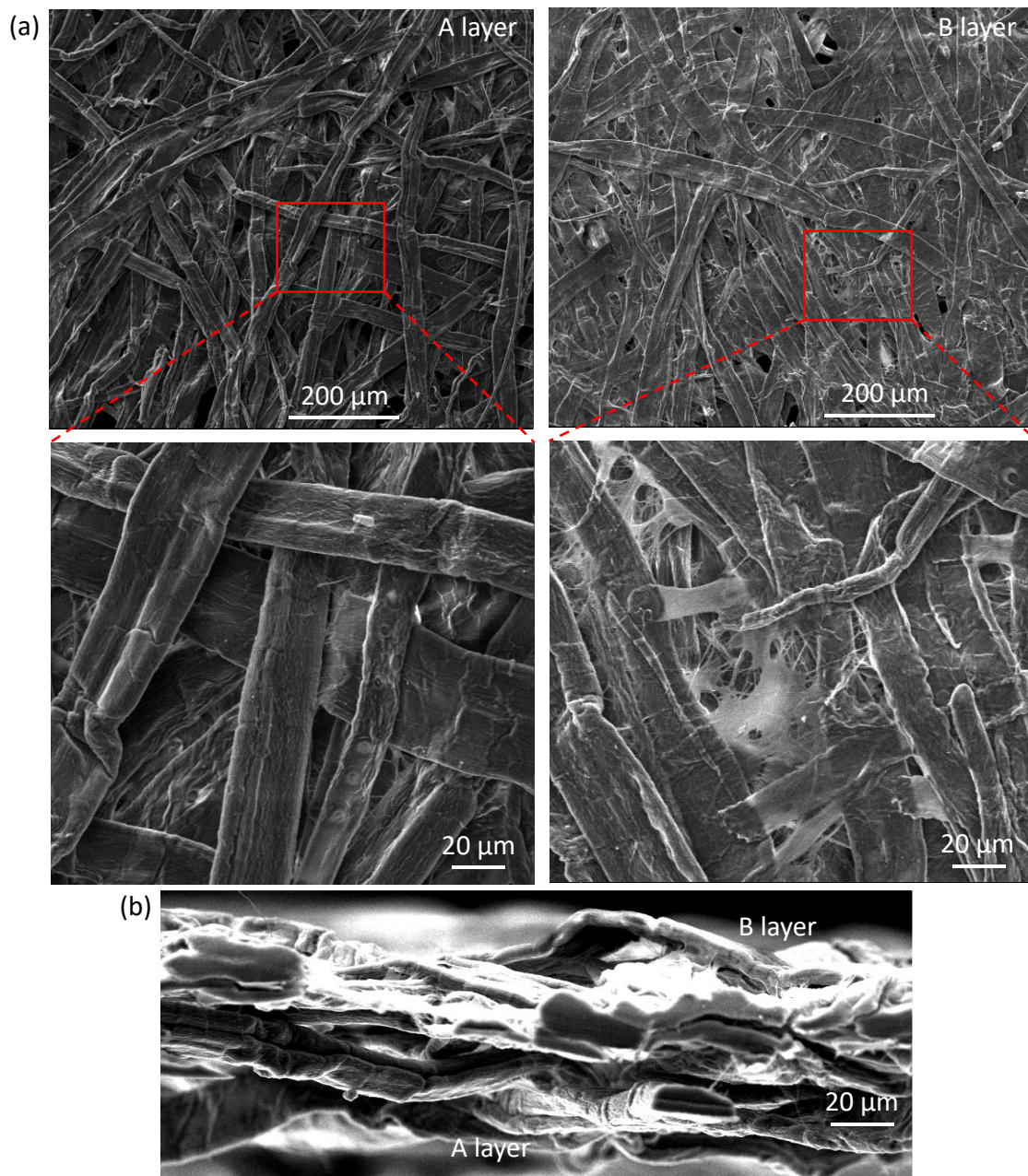
256

257 **Table 3.** Physical Properties of the two stratified papers made under (wet) unpressed (UP) or
 258 pressed (P) conditions. °() Estimations of the σ_{break} using a two-layer parallel model, by

259 averaging the σ_{break} of the A fraction paper and the B fraction paper, taking into account the
 260 respective thickness of each layer.

Paper Properties		Monolayered		Stratified 1		Stratified 2	
		Native		A/B (50%/50%)		LFA+SFA/LFB+SFB (84.5%/15.5%)	
		UP	P	UP	P	UP	P
Basis weight (g/m ²)		21.3 ±0.2	21.6 ±0.2	22.1 ±0.2	22.4 ±0.2	20.2 ±0.9	21.7 ±0.6
Thickness (µm)		187 ±5	73 ±3	158 ±5	84 ±5	185 ±14	80 ±8
Density (kg/m ³)		114 ±4	297 ±14	140 ±7	267 ±9	109 ±6	273 ±28
Apparent Young's Modulus E (GPa)	MD	0.19 ±0.04	0.70 ±0.10	0.33 ±0.08	0.83 ±0.10	0.16 ±0.04	0.62 ±0.10
	CD	0.05 ±0.01	0.38 ±0.08	0.10 ±0.01	0.25 ±0.05	0.08 ±0.01	0.24 ±0.06
Tensile breaking stress σ_{break} (MPa)	MD	1.84 ±0.12	9.01 ±0.67	4.63 ±0.41 °(3.40)	13.60 ±0.73 °(12.74)	2.02 ±0.12	9.08 ±0.45
	CD	0.67 ±0.05	3.03 ±0.25	1.13 ±0.04 °(0.84)	3.78 ±0.30 °(3.96)	0.79 ±0.02	3.01 ±0.12
Strain at break ϵ_{break} (%)	MD	3.6 ±0.8	5.4 ±1.3	4.3 ±0.9	5.2 ±0.1	3.3 ±0.3	4.1 ±0.4
	CD	3.8 ±0.6	4.6 ±0.4	3.5 ±0.3	5.1 ±0.3	2.5 ±0.2	3.7 ±0.5

261
 262



263

264 **Fig. 4** FESEM micrographs of Stratified 1(A/B) paper: (a) A and B surfaces, and (b) cross section.

265

3.2. Mechanical properties of model papers

266

267

268

269

270

271

272

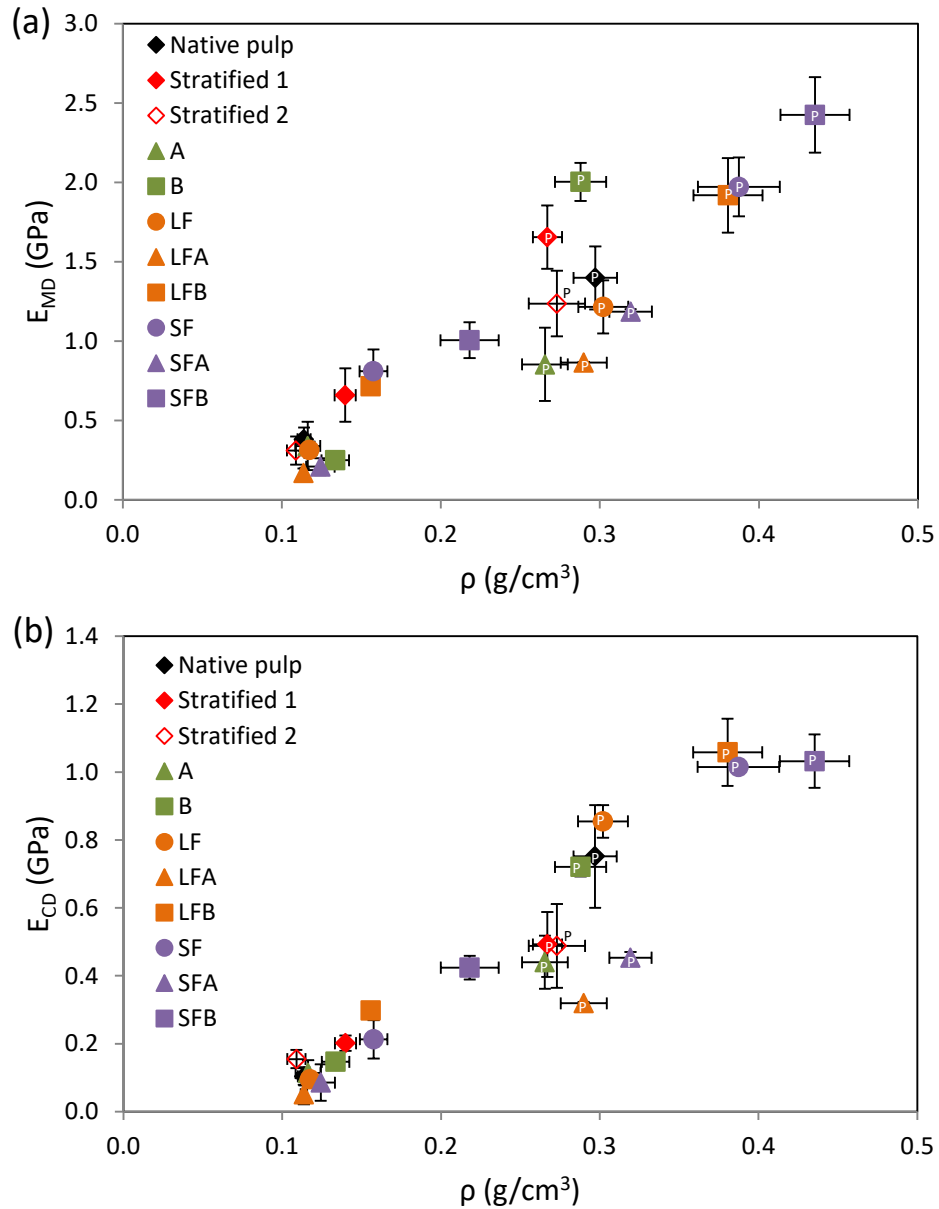
273

The profiles of the stress-strain curves were quite similar across different model papers (Fig. 2). Initially, the curves exhibited a linear relationship between stress and strain, reflecting the material's elastic behavior. After reaching the yield point, stress continued to increase, albeit with a reduced slope, until the breaking point (represented as a star in Fig. 2a). As expected, the curve typically shows a steeper slope in the MD compared to the CD and tends to gradually flatten as the paper deforms in the CD. In the following, the mechanical behavior of all model papers is compared based on the slope in the linear region, reflecting the apparent Young's modulus (E), the tensile breaking stress (σ_{break}) and the strain at break (ε_{break}).

274 **Figures 5a and 5b** depict the evolution of **apparent** Young's modulus with the paper
 275 density along the machine direction MD and cross direction CD, respectively. Notably, due to
 276 the used processing route which induced preferred fiber orientation along MD, the **apparent**
 277 Young modulus was observed to be around twice as high in MD compared to CD, whatever the
 278 considered paper. Firstly, the elastic moduli exhibited an overall increase with the paper density
 279 which is a well-known trend. At fixed paper formulation and whatever the considered
 280 formulation, this is emphasized by closely looking at investigated pressing conditions: the
 281 higher the normal stress during the forming phase, the higher the number of fiber-fiber contacts,
 282 the higher the contact surfaces (and thus the relative bonded area *RBA*) and the higher the
 283 Young's moduli (Marulier et al. 2015, Orgéas et al. 2021). However, some differences arise
 284 among the studied papers. At fixed pressing condition, these differences may be induced by the
 285 fiber aspect ratio l/w as well as the relative bonded area *RBA* (Page and Seth 1980, Orgéas et
 286 al. 2021). For example, following Page and Seth, the Young modulus E_p of an in-plane isotropic
 287 paper fiber network is a function of the fiber volume fraction ϕ , the fiber aspect ratio l/w , and
 288 the *RBA* as follows:

$$289 \quad E_p = \frac{1}{3} E_f \Phi \left(1 - \frac{1}{\frac{l}{w} RBA} \sqrt{\frac{E_f}{2G_f}} \right) \quad (1)$$

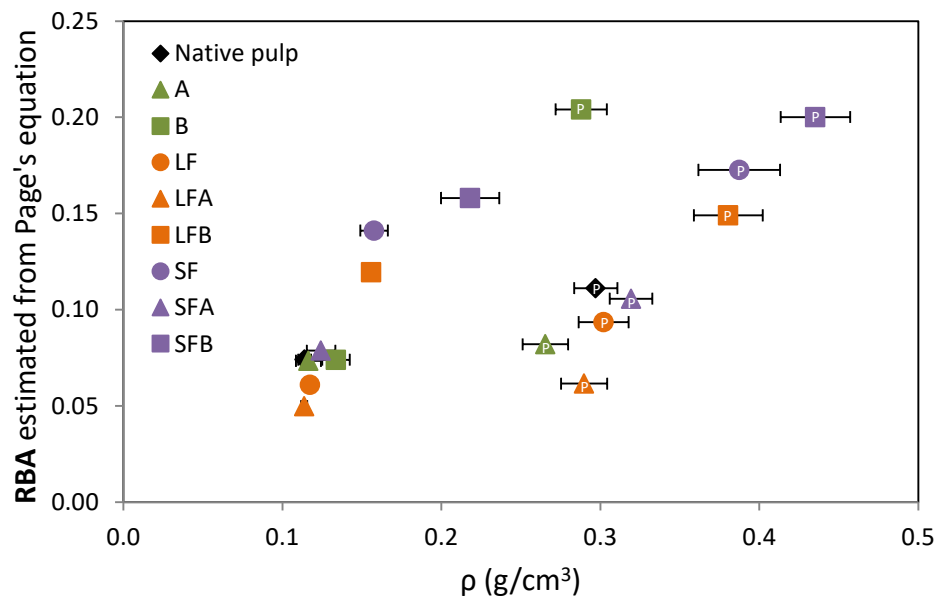
290
 291 Where E_f and G_f are the fiber Young's and shear moduli, respectively. In the following
 292 these quantities were assumed constant regardless of fiber morphology, for the sake of
 293 simplicity. Eq. (1) shows that at given fiber volume fraction, the higher the fiber aspect ratio
 294 l/w or the *RBA*, the higher the Young modulus, with a limit which tends to that predicted by the
 295 Cox model (Cox 1952).



296
 297 **Fig. 5** Apparent Young's moduli E_{MD} (a) and E_{CD} (b) as functions of the paper density ρ for all model
 298 papers along the machine (a) and cross (b) directions. Marks with a letter "P" indicate papers that were
 299 pressed upon processing.

300 As evident from Fig. 5, the model papers originating from the apex fiber fractions
 301 occupy the lower part of the cloud of experimental points, whereas those from the base fiber
 302 fractions were situated in the upper part. Meanwhile, the fiber aspect ratio l/w is higher for the
 303 apex fraction papers (refer to Tables 1 and 2). Therefore, according to Eq. (1), the evolution of
 304 this parameter alone cannot elucidate the observed difference in the evolution of apparent
 305 Young's moduli with paper density between apex and base fraction papers. It is more likely that
 306 the RBA could play a dominant role in this regard. The RBA was anticipated to be notably higher

307 for the base fraction papers due to their concentration of highly fibrillated fibers and fines. To
 308 verify this assumption, we estimated the *RBA* using Eq. (1) for all the monolayered model
 309 papers. For that purpose, the Young's modulus E_p was calculated as the mean value between
 310 the MD and CD, with E_f and G_f set to 30 GPa and 3 GPa respectively, *i.e.*, reasonable estimates
 311 for softwood fibers (Mansour et al. 2019, Orgéas et al. 2021). The resulting values of the *RBA*
 312 are reported in Tables 1 and 2, and plotted as functions of the paper densities in **Figure 6**. It is
 313 worth noting that this estimated *RBA* should not be considered strictly as a quantification
 314 parameter; rather, it should only be used as a tool for comparing papers in terms of degree of
 315 bonding.

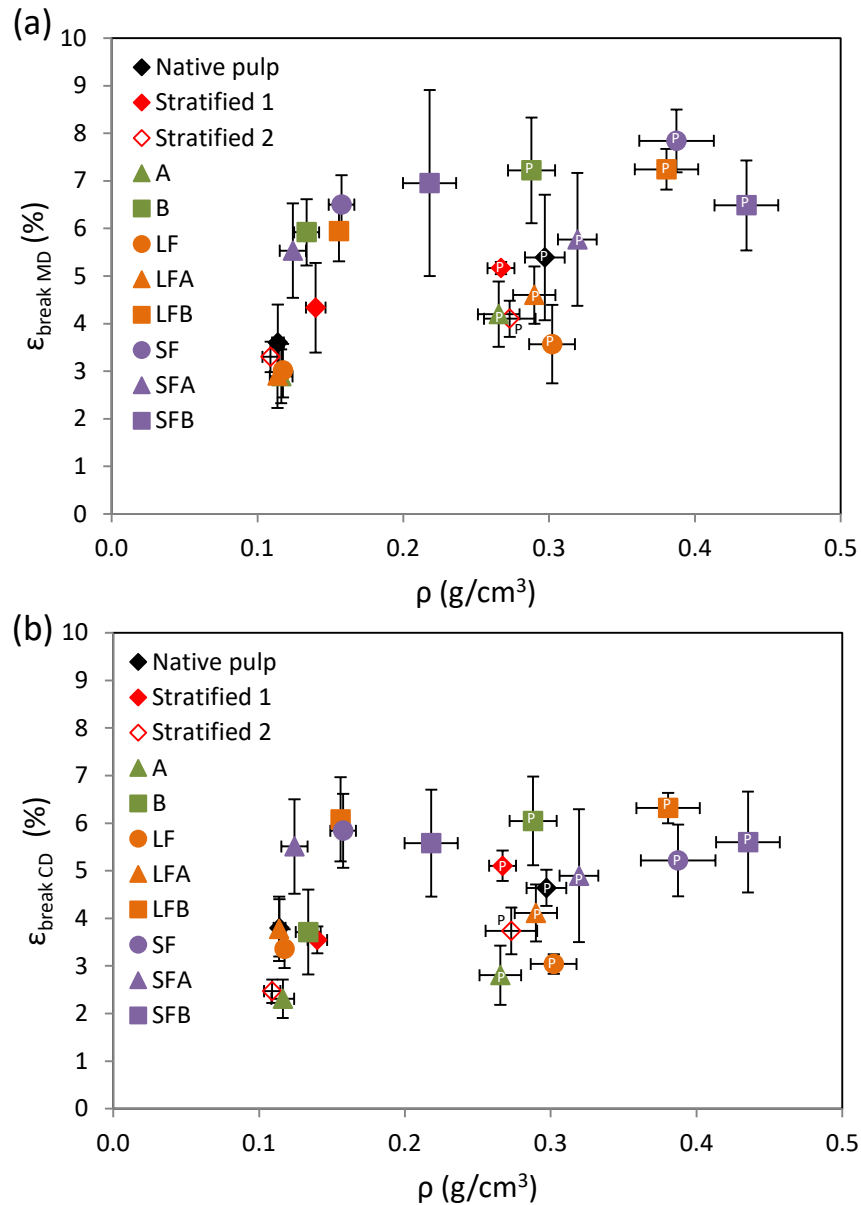


316
 317 **Fig. 6** Relative Bonded Area *RBA* estimated from Eq. (1) as a function of paper density ρ for all the
 318 monolayered model papers. Marks with a letter “P” indicate papers that were pressed upon processing.

319 As revealed by **Figure 6**, the *RBA* values exhibit significant variations among the
 320 different model papers and forming conditions. Firstly, for unpressed papers, *i.e.*, for identical
 321 pressing condition, the increase of the *RBA* with the paper density is noticeable, with, the lowest
 322 values for LFA, with slightly higher values for LF, then for apex fractions SFA and A, and with
 323 considerably higher values for SF and base fractions LFB, B, and SFB (up to four times higher
 324 than LFA for SFB). Interestingly, this ranking well correlates with the fibrillation index and
 325 fine content: the higher the values of these parameters, the higher the *RBA*. This relationship is
 326 expected, as the fibrillation index is associated with the specific surface area of fibers, which,
 327 along with the presence of fines, plays a pivotal role in bonding development. Notably, the
 328 native paper was situated in the upper part of the apex fraction group. In addition, it is worth

329 noting that for a given model paper, increasing the normal pressing stress during paper forming
330 induces an important increase of the paper density but also a noticeable increase of its RBA
331 (Marulier et al. 2015, Orgéas et al. 2021).

332 **Figure 7** illustrates the evolution of **strain at break** ϵ_{break} with paper density. ϵ_{break} is
333 relatively equivalent in the MD and CD across all papers. This could be attributed to the specific
334 drying conditions (air-dried and sandwiched between PVC plates along the long edges).
335 However, ϵ_{break} depends on the considered fractions, albeit showing only a slight
336 dependency/increase with the paper density (at fixed fraction). **At fixed pressing condition, two**
337 **distinct groups emerged: LF and apex fraction papers, which reached values between 3% and**
338 **5%, and SF and base fraction papers, which reached values around 6-7%.** This trend appears to
339 correlate well with the fibrillation index and fine content, and consequently, with RBA: higher
340 values of these parameters corresponded to higher **strain at break**. The deformability of low-
341 density papers is known to largely depend on the bonding between fibers: the higher the
342 bonding efficiency, the greater the **strain at break** (Vishtal and Retulainen 2014, Kouko et al.
343 2020). Notably, the native paper and the stratified papers occupied intermediate positions
344 between the two groups. **Note that the strain at break values in this study differ from those of**
345 **industrial tissue papers, which typically exhibit higher values in the machine direction due to**
346 **the creping process. It will be important to verify whether the differences between fractions**
347 **remain consistent after the creping process.**



348

349 **Fig. 7** Strain at break ϵ_{break} as a function of the paper density ρ for all model papers in the (a) machine
 350 direction MD and (b) cross direction CD. Marks with a letter “P” indicate papers that were pressed upon
 351 processing.

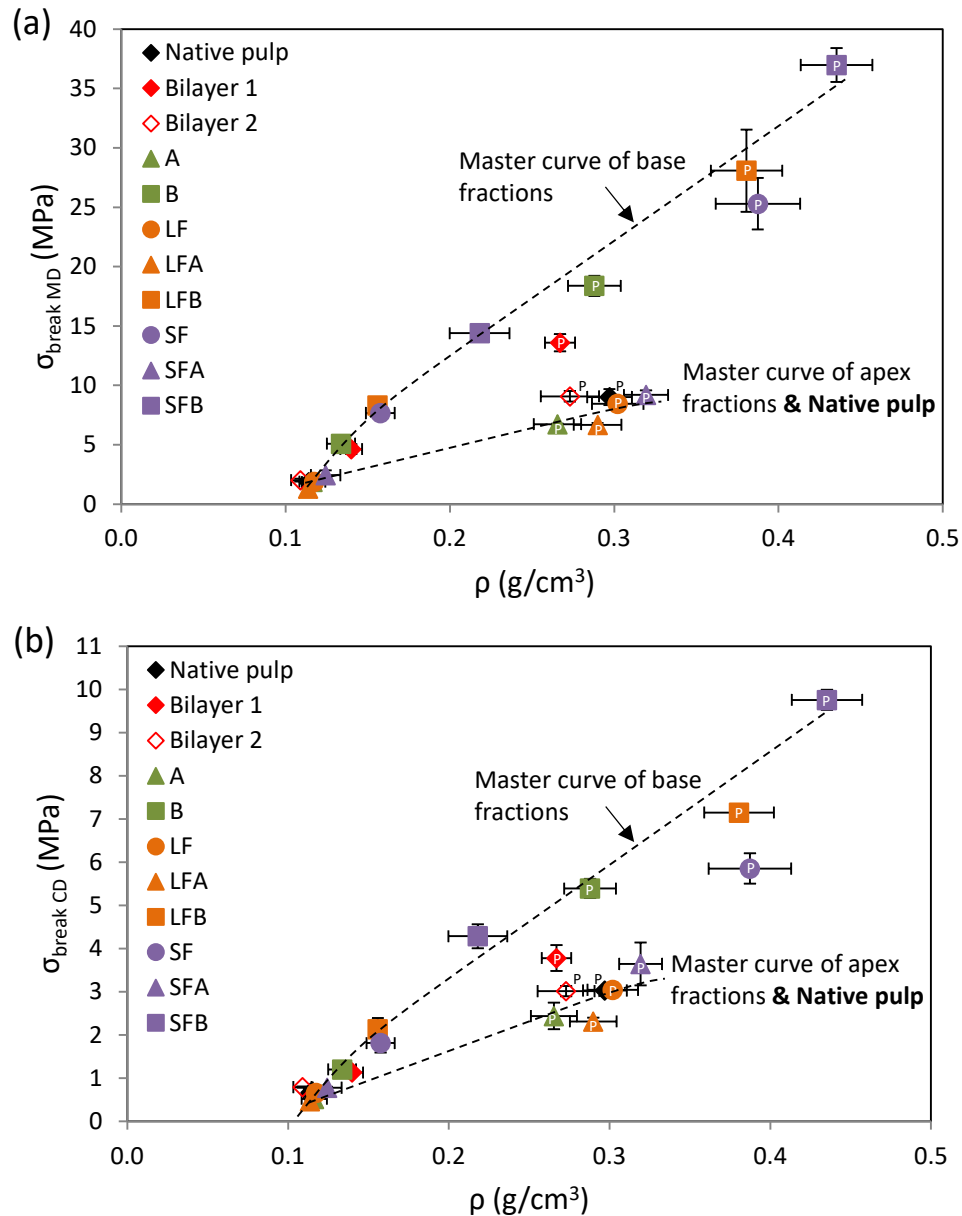
352 **Figures 8a and 8b** show the evolution of the **tensile breaking stress** σ_{break} of model papers
 353 with paper density, along the MD and CD, respectively. These results emphasize a well-known
 354 trend, whatever the fraction and the forming condition: the higher the paper density, the higher
 355 the number and the surface of contacts between particles (fibers, fines, fibrils), and thus the
 356 higher the stress levels required to damage and break the paper. Interestingly, papers from the
 357 base fractions and apex fractions follow two distinct curves. The **breaking stress** σ_{break} of base
 358 fraction papers exhibit a strong increase with paper density, whereas this property for apex

359 fraction papers increased more gradually. For example, at a density of 0.3 g/cm³, the σ_{break} of
360 base fraction papers is at least twice that of apex fraction papers. This difference may be
361 attributed to the higher level of fiber-to-fiber bonding in base fraction papers, as suggested by
362 the estimated RBA reported in Fig. 6. Fibrils and fines bridges which were formed between
363 fibers in base fraction papers, as observed in Fig. 4, contribute to carry the tensile load and to
364 reduce stress concentrations in bonded regions (Motamedian et al. 2019). Also, it is noteworthy
365 that LF papers tend to align with the master curve of apex fraction papers, while SF papers tend
366 to align with the master curve of base fraction papers. This alignment was expected, as the short
367 fiber fraction concentrates more fibrillated fibers and fines.

368 Interestingly, Stratified 1 papers occupied an intermediate position between the two
369 aforementioned master curves (Fig. 8), while the σ_{break} of native papers tended to align with the
370 master curve of apex fraction papers. Ultimately, the σ_{break} of Stratified 1 paper surpassed that
371 of both native and apex fraction papers by approximately 60% according to the master curve
372 analysis. This improvement underscores the effectiveness of stratification in overcoming the
373 alignment of native paper behavior with that of apex fraction papers. It is worth mentioning that
374 Stratified 2 papers remained within the same range as native papers, likely due to the
375 distribution of each fraction in the stratified structure (84.5% apex fraction fibers and 15.5%
376 base fraction fibers.

377

378



379

380 **Fig. 8** Evolution of the **tensile breaking stress** σ_{break} with the paper density ρ for all model papers along
 381 the machine (a) and cross (b) directions. Marks with a letter "P" indicate papers that were pressed upon
 382 processing.

383 As previously mentioned, the native paper web can be regarded as a blend of stiff, low-
 384 fibrillated fibers and conformable, fibrillated fibers. The mechanical behavior of this web might
 385 differ from the average behavior of both the apex fraction paper and the base fraction paper.
 386 This difference arises because the development of bonding between fibers may be constrained
 387 by the stiffer, low-fibrillated fibers (Fernandez and Young 1994, Niskanen and Kärenlampi
 388 1998). In this context, the stiff and low-fibrillated fibers could dictate the in-plane mechanical
 389 behavior of the native papers, resulting in behavior akin to that of apex fraction papers.

390 However, by stratifying the sheet, the paper's mechanical performance was no longer hindered
391 by the stiff, low-fibrillated fibers. Two webs, each approximately 10 g/m² and with relatively
392 independent structural and mechanical properties, were superimposed (see Figure 4c). This
393 hypothesis on the relative independency is supported by the estimations of σ_{break} using a two-
394 layer parallel model based on the Voigt approximation (Aboudi 2013), as presented in Table 3
395 under “e”, which are rather close to the experimental values.

396
397

CONCLUSIONS

398 In this experimental study, we investigated the potential of stratified forming combined with
399 pulp fractionation to improve the mechanical strength of 20 g/m² model papers made from
400 softwood kraft pulp. Pulp fractionation enabled the separation of fibers based on their
401 morphology, fibrillation degree and fine content, resulting in papers with distinct mechanical
402 behaviors. Regarding the strain at break ϵ_{break} and breaking stress σ_{break} , two distinct groups of
403 papers emerged: papers made from short and/or flexible highly fibrillated fibers containing
404 fines (B) and papers made from long and/or stiff low-fibrillated fibers (A). The breaking stress
405 of B papers exhibited a strong increase with paper density whereas this property for A papers
406 increased more gradually. Finally, at a density of 0.3 g/cm³, the values σ_{break} of B papers is at
407 least twice that of A papers. The strain at break of B papers was close to two times higher than
408 that recorded for A papers albeit showing only a slight dependency/increase with the paper
409 density. This difference was primarily attributed to the level of fiber-to-fiber bonding, which is
410 related to the specific surface area provided by fibrillated fibers and the presence of fines, both
411 of which play a pivotal role in bonding development. Interestingly, regarding the breaking stress
412 of the bilayer papers (A/B) were in an intermediate position between the two aforementioned
413 trends while the native pulp paper (*i.e.*, without fractionation and stratified forming) followed
414 the trend of A papers. As a result, bi-layering the paper improved σ_{break} up to twice as much
415 without increasing the paper density. Since densification directly impacts the absorbency and
416 softness of tissue paper, this approach could significantly improve the balance of properties
417 across different tissue paper grades. Further investigations are required to quantify how this
418 method influences these properties, as well as wet strength. Additionally, it is essential to assess
419 whether the improvements in property balance are maintained after the creping process and to
420 understand how stratification may affect the creping process itself. Finally, evaluating the
421 potential of this method with hardwood or eucalyptus fiber pulps would be highly valuable.

422 **ACKNOWLEDGMENTS**

423

424 The authors acknowledge the financial support from CTP and CTPi Members. Christian
425 Berek, Priscilla Marquet, Mélanie Lehmann and Xavier Rousset are thanked for experimental
426 work. LGP2 and 3SR Lab are part of the LabEx Tec 21 and the Carnot Institute Polynat.

427

428 **REFERENCES CITED**

429 **Aboudi, J. (2013). *Mechanics of composite materials: a unified micromechanical approach.***
430 ***Elsevier.***

431 Bergström, J. (2006). *Flow field and fiber fractionation studies in hydrocyclones* (Doctoral
432 dissertation, KTH).

433 Cox, H. L. (1952). The elasticity and strength of paper and other fibrous materials. *British*
434 *journal of applied physics*, 3(3), 72.

435 De Assis, T., Reisinger, L. W., Pal, L., Pawlak, J., Jameel, H., and Gonzalez, R. W. (2018).
436 “Understanding the effect of machine technology and cellulosic fibers on tissue
437 properties—A review,” *BioResources* 13(2), 4593-4629.

438 De Assis, T., Pawlak, J., Pal, L., Jameel, H., Reisinger, L. W., Kavalew, D., Campbell, C.,
439 Pawlowska, L., and Gonzalez, R. W. (2020). “Comparison between uncreped and creped
440 handsheets on tissue paper properties using a creping simulator unit,” *Cellulose* 27(10),
441 5981-5999. <https://doi.org/10.1007/s10570-020-03163-0>

442 Fernandez, E. O., and Young, R. A. (1994). “An explanation for the deviation from linearity
443 in properties of blends of mechanical and chemical pulps,” *Tappi Journal* 77(3), 221-224.

444 Gigac, J., and Fišerová, M. (2008). “Influence of pulp refining on tissue paper properties,”
445 *Tappi Journal* 7(8), 27-32.

446 Harwood, J. W. (1990). “Stratification of paper grades.” *Tappi journal* 73(5), 115-122.

447 Hirn, U., and Schennach, R. (2015). “Comprehensive analysis of individual pulp fiber bonds
448 quantifies the mechanisms of fiber bonding in paper,” *Scientific Reports* 5(1), 1-9.
449 <https://doi.org/10.1038/srep10503>

450 Huber, P., Carré, B., Fabry, B., & Kumar, S. (2013). Optimizing stratified forming for light-
451 weight coated paper grades made from deinked pulp fractions. *Nordic Pulp & Paper*
452 *Research Journal*, 28(2), 302-312. <https://doi.org/10.3183/npprj-2013-28-02-p302-312>

453 Huber, P., Carré, B., Kumar, S., and Lecourt, M. (2018). “Optimum strategies for pulp
454 fractions refining,” *Nordic Pulp and Paper Research Journal* 33(1), 3-11.
455 <https://doi.org/10.1515/npprj-2018-3012>

456

457 Kouko, J., Turpeinen, T., Kulachenko, A., Hirn, U., & Retulainen, E. (2020). Understanding
458 extensibility of paper: role of fiber elongation and fiber bonding. *Tappi J*, 19(3), 125-135.

459 Kullander, J., Nilsson, L., and Barbier, C. (2012). “Evaluation of furnishes for tissue
460 manufacturing; suction box dewatering and paper testing,” *Nordic Pulp and Paper
461 Research Journal* 27(1), 143-150. <https://doi.org/10.3183/npprj-2012-27-01-p143-150>

462 Lindström, T., Fellers, C., Ankerfors, M., & Glad-Nordmark, G. (2014). On the strength
463 mechanism of dry strengthening of paper with nanocellulose. *Proceedings of the Recent
464 Advances in Cellulose Nanotechnology Research: Production, Characterization and
465 Applications, Trondheim, Norway.*

466 Lloyd, M. (2000). Stratified (multilayer) forming: a technology for the new millennium?.
467 *Appita journal*, 53(3), 188-194.

468 **Morais, F. P., Carta, A. M. M., Amaral, M. E., & Curto, J. M. (2021a). Cellulose fiber
469 enzymatic modification to improve the softness, strength, and absorption properties of
470 tissue papers. *BioResources*, 16(1), 846.**

471 Morais, F. P., Carta, A. M., Amaral, M. E., and Curto, J. M. (2021b). “Micro/nano-fibrillated
472 cellulose (MFC/NFC) fibers as an additive to maximize eucalyptus fibers on tissue paper
473 production,” *Cellulose* 1-19. <https://doi.org/10.1007/s10570-021-03912-9>

474 Motamedian, H. R., Halilovic, A. E., & Kulachenko, A. (2019). Mechanisms of strength and
475 stiffness improvement of paper after PFI refining with a focus on the effect of fines.
476 *Cellulose*, 26(6), 4099-4124. <https://doi.org/10.1007/s10570-019-02349-5>

477 Niskanen, K., & Kärenlampi, P. (1998). In-plane tensile properties. *Paper physics*, 16, 172.

478 Niskanen, K. (Ed.). (2011). *Mechanics of paper products*. Walter de Gruyter.

479 Orgéas, L., Dumont, P. J., Martoia, F., Marulier, C., Le Corre, S., & Caillerie, D. (2021). On
480 the role of fiber bonds on the elasticity of low-density papers: a micro-mechanical
481 approach. *Cellulose*, 28(15), 9919-9941. <https://doi.org/10.1007/s10570-021-04098-w>

482 **Oksanen, A., Salminen, K., Kouko, J., & Retulainen, E. (2012). The effects of TMP and filler
483 stratifying on wet web runnability and end product quality of fine paper. *Nordic Pulp &
484 Paper Research Journal*, 27(1), 130-136.**

485 Page DH, Seth RS (1980) The elastic modulus of paper. II: The importance of fiber modulus,
486 bonding, and fiber length. *Tappi* 63:113–116.

487 Steadman, R., and Luner, P. (1985). “The effect of wet fiber flexibility on sheet apparent
488 density,” *Papermaking Raw Materials* 1, 311-337.

489 Vieira, J. C., de Oliveira Mendes, A., Carta, A. M., Galli, E., Fiadeiro, P. T., & Costa, A. P.
490 (2020). Impact of embossing on liquid absorption of toilet tissue papers. *BioResources*,
491 15(2), 3888.

492 Vigié, J., Kumar, S., & Carré, B. (2022). A Comparative Study of the Effects of Pulp
493 Fractionation, Refining, and Microfibrillated Cellulose Addition on Tissue Paper
494 Properties. *BioResources*, 17(1), 1507-1517.

495 Vishtal, A., & Retulainen, E. (2014). Boosting the extensibility potential of fiber networks: A
496 review. *BioResources*, 9(4), 7951-8001.

497 Wang, Y. (2019). *The physical aspects of softness perception and its relationship to tissue*
498 *paper properties. North Carolina State University*

499 Wohlert, M., Bensselfelt, T., Wågberg, L., Furó, I., Berglund, L. A., & Wohlert, J. (2021).
500 Cellulose and the role of hydrogen bonds: not in charge of everything. *Cellulose*, 1-23.
501 <https://doi.org/10.1007/s10570-021-04325-4>

502 Zambrano, F., Wang, Y., Zwilling, J. D., Venditti, R., Jameel, H., Rojas, O., and Gonzalez, R.
503 (2021). “Micro-and nanofibrillated cellulose from virgin and recycled fibers: A
504 comparative study of its effects on the properties of hygiene tissue paper,” *Carbohydrate*
505 *Polymers* 254, article no. 117430. <https://doi.org/10.1016/j.carbpol.2020.117430>
506